

# Complementary Advantages: Exploiting Cross-Field Frequency Correlation for NIR-Assisted Image Denoising

Yuchen Wang<sup>1</sup> Hongyuan Wang<sup>1</sup> Lizhi Wang<sup>2\*</sup>  
 Xin Wang<sup>1</sup> Lin Zhu<sup>1</sup> Wanxuan Lu<sup>3</sup> Hua Huang<sup>2</sup>

<sup>1</sup>Beijing Institute of Technology <sup>2</sup> Beijing Normal University <sup>3</sup> Chinese Academy of Sciences

## Abstract

Existing single-image denoising algorithms often struggle to restore details when dealing with complex noisy images. The introduction of near-infrared (NIR) images offers new possibilities for RGB image denoising. However, due to the inconsistency between NIR and RGB images, the existing works still struggle to balance the contributions of two fields in the process of image fusion. In response to this, in this paper, we develop a cross-field Frequency Correlation Exploiting Network (FCENet) for NIR-assisted image denoising. We first propose the frequency correlation prior based on an in-depth statistical frequency analysis of NIR-RGB image pairs. The prior reveals the complementary correlation of NIR and RGB images in the frequency domain. Leveraging frequency correlation prior, we then establish a frequency learning framework composed of Frequency Dynamic Selection Mechanism (FDSM) and Frequency Exhaustive Fusion Mechanism (FEFM). FDSM dynamically selects complementary information from NIR and RGB images in the frequency domain, and FEFM strengthens the control of common and differential features during the fusion of NIR and RGB features. Extensive experiments on simulated and real data validate that our method outperforms various state-of-the-art methods in terms of image quality and computational efficiency. The code will be released to the public.

## 1. Introduction

Due to the inherent physical limitations of digital imaging devices, the captured images are often affected by various types of noise, which have a significant impact on applications such as 24-hour surveillance, autonomous driving, and smartphone photography. Restoring clean detailed information from noisy images that lack substantial information is highly ill-posed. Although the development of deep learning techniques [20, 31] that have brought forth a vari-

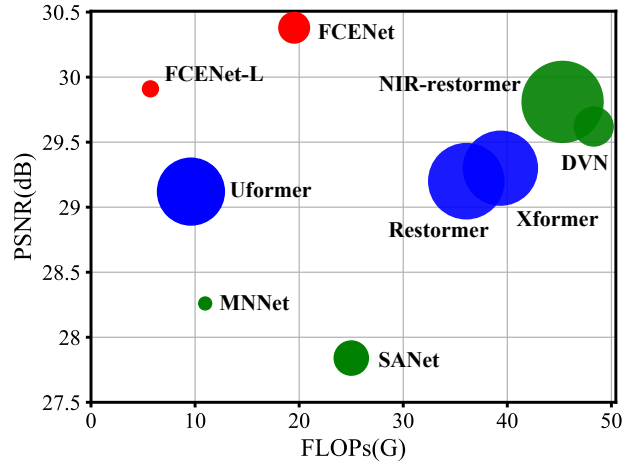


Figure 1. Comparisons of PSNR, FLOPs, and Parameters on the DVD dataset [16] are presented. Green circles represent the single-image denoising algorithm, and blue circles represent the NIR-assisted image denoising algorithm. The circle radius represents the number of parameters. Our method (red circles) achieves the superior performance while maintaining efficiency.

ety of image denoising methods [1, 12, 43, 47], existing algorithms still struggle to restore details when dealing with complex noisy images, especially in low-light environment. Therefore, it is necessary to introduce supplementary information from new fields. Fortunately, the introduction of near-infrared (NIR) images offers new possibilities for image denoising. NIR images with high Signal to Noise Ratio (SNR) can be captured at a low cost and is suitable for everyday photography. Thus, NIR-assisted image denoising [22, 32, 42] has become a promising solution for image denoising.

However, it is challenging to effectively leverage information from different fields to achieve noise reduction. Due to the influence of the inherent reflective spectra of objects, there are inconsistencies between NIR and RGB images. As shown in Fig. 2, firstly, there is a significant difference in color and brightness information between two fields. Secondly, some structural texture of RGB image disappears

\*Corresponding Author: Lizhi Wang (wanglizhi@bnu.edu.cn)

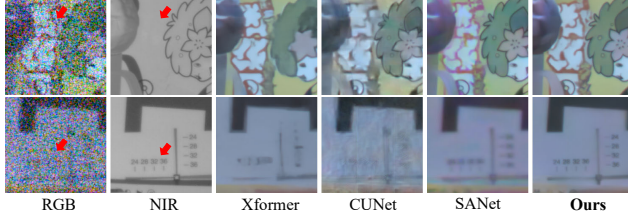


Figure 2. Superiority of our method. Visual comparisons on a challenging noisy RGB-NIR image pair. Pay attention to the differences in structural and color information between two fields. Our method produces a better denoising result with clear details and fewer artifacts.

in NIR image, and additional artifacts may appear. The color and structural inconsistencies between NIR and RGB images pose a significant challenge for the task of NIR-assisted image denoising.

In existing research, Some methods attempt to directly integrate inconsistent features from two fields [26, 27, 38, 39]. However, these methods indiscriminately fuse cross-field information, relying on the fitting capabilities of neural networks to learn the fusion of NIR and RGB images under spatial inconsistency, which often leads to suboptimal denoising results and lower computational efficiency.

Some methods reinforce common features from NIR and RGB images and diminish the weight of inconsistent features during the fusion [10, 16, 17, 42]. These image fusion schemes typically only enhance the common information in NIR and RGB during fusion, but some differential information such as the sharp textures in NIR and the color information in RGB are discarded. In this paper, we developed an cross-field Frequency Correlation Exploiting Network (FCENet) for NIR-assisted image denoising. We conduct a series of analyses on the characteristics of NIR and RGB images in the frequency domain and obtain a key observation: in the same scene, the similarity between noisy RGB images and clean RGB images decreases from low to high frequency, whereas the similarity between NIR images and clean RGB images increases from low to high frequency. This significant cross-field frequency correlation prior provide us with inspiration, prompting us to subsequently establish detailed frequency domain learning to thoroughly excavate complementary information from NIR and RGB images.

Specifically, our frequency domain fusion network consists of two mechanisms: The Frequency Dynamic Selection Mechanism (FDSM) and Frequency Exhaustive Fusion Mechanism (FEFM). In order to comprehensively extract useful features from inconsistent images, we formulate the FDSM based on dynamic filters guided by the results observed in the frequency domain. The FDSM efficiently screens complementary features from NIR and RGB in the frequency domain, providing high quality material for subsequent image fusion. Then, to ensure thorough fre-

quency domain fusion, we innovatively formulate FEFM. In FEFM, for the common and differential features in the NIR and RGB feature maps output by FDSM, we simultaneously model local and long-range correlations across fields to fully model the common features from cross-field information, and employ a differential cross-attention approach to complement some key differential high frequency features in NIR. Our contributions are summarized as follows:

- We establish the frequency correlation prior between NIR and RGB images through a series of frequency domain analyses of two fields, which prompt the implementation of integrating complementary features in the frequency domain.
- We propose an efficient frequency dynamic selection mechanism on the basis of the frequency correlation prior to identify which useful low-frequency and high frequency information should be retained in NIR and RGB features.
- We develop an exhaustive frequency domain fusion mechanism that models the local similarity and long-range correlation in the frequency domain of NIR and RGB images, and supplements some critical high frequency differential features.
- Extensive experiments on simulated and real data validate that our method outperforms various state-of-the-art (SOTA) methods in terms of image quality and computational efficiency.

## 2. Related Work

### 2.1. Single Image Denoising

Image denoising [19, 30] is a classic task in low-level vision. In recent years, the theory of deep learning has greatly improved the accuracy and efficiency of denoising [1, 2, 6, 36]. DnCNN [46] uses a simple network with batch normalization and residual learning, which outperforms traditional denoising methods. MPRNet [43] designed a multi-stage restoration framework, and Restormer [44] proposed an efficient transformer framework for high-resolution images. Xformer [45] proposed a transformer framework that combines spatial self-attention and channel self-attention. However, despite their strong denoising capabilities, single-image denoising still inevitably loses a lot of spatial information, leading to overly smooth edge textures in the denoised images.

### 2.2. NIR-assited Image Restoration

To achieve better denoising effects, researchers have attempted to use near-infrared (NIR) images to assist in RGB image denoising [7, 22, 33, 42]. Compared with single-image recovery, NIR images can help restore the details of degraded images [32, 38]. In early research, Yan et

al. [42] proposed a Scale Map from the perspective of gradient inconsistency to find universal usable edges and smooth transitions in NIR images. With the widespread application of deep learning methods, CUNet [10] uses a convolutional sparse coding model to extract common features from cross-field images. FGDNet [26] and SANet [27] fuse the features of two fields in the frequency domain. MNNet [39] proposed an observation model that takes into account the modality gap between the target and guiding images. DVN [16] integrates structural inconsistency priors into deep features, specifically strengthening the common deep features in NIR and RGB. NAID [38] proposed an efficient Selective Fusion Module (SFM), which can be plugged into advanced image restoration networks. However, when confronted with dense noise in extreme environments, most existing NIR-assisted image denoising methods struggle to achieve a balance between color restoration, detail preservation, and artifact suppression under inconsistency.

### 2.3. Frequency Domain Image Restoration

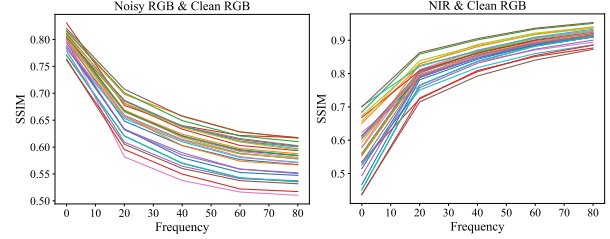
Frequency analysis in digital signal processing emphasizes the frequency properties of signals [24, 28, 40]. Recently, frequency domain analysis has shown great potential in improving the performance of various learning-based image restoration frameworks [15, 37, 41, 49]. In [18], An efficient estimation of scaled dot-product attention based on a frequency domain self-attention solver (FSAS) was proposed. HDNet [14] proposed a high-resolution dual-domain learning network. SFNet [9] uses filters to dynamically decouple feature mappings into different frequency components and adaptively extract useful features. In this paper, we emphasize the importance of frequency domain information for the research on fusion under RGB/NIR inconsistency and design a comprehensive frequency domain fusion scheme for this task to ensure the utilization of complementary information from NIR and RGB images.

## 3. Method

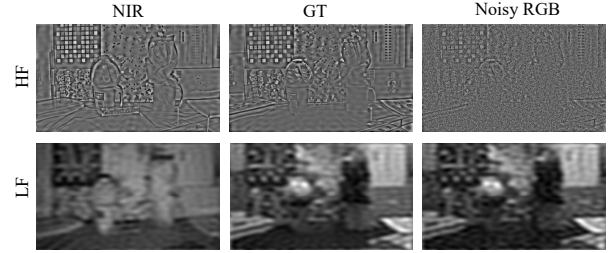
In this section, we first introduce the cross-field frequency correlation prior of NIR and RGB images. Based on the cross-field frequency correlation priors, we formulate a detailed frequency domain scheme, including the Frequency Dynamic Selection Mechanism (FDSM) and the Frequency Exhaustive Fusion Mechanism (FEFM) for thorough frequency exploitation.

### 3.1. Cross-field Frequency Correlation Prior

To address the fusion of NIR and RGB images under spatial inconsistency, it is imperative to distinguish which information in NIR and RGB images is useful and which is redundant or even erroneous for denoising. We randomly select 30 pairs of NIR images, noisy RGB images, and clean RGB



(a) Frequency Correlation between NIR and RGB



(b) Visualization Results after Filtering

Figure 3. The analysis of NIR and RGB frequency correlation. (a) The left graph represents the frequency correlation between noisy RGB and clean RGB and the right graph represents the frequency correlation between near-infrared images and clean RGB, with the horizontal axis indicating the cutoff frequency of the high-pass filter. Different colored curves represent different scenarios. (b) The visualization results of images output by a fixed frequency filter, with the first row showing high frequency (HF) part and the second row showing low frequency (LF) part.

images from the existing RGB-NIR dataset and performed Fourier Transform on them. To facilitate the study of the correlation between NIR and RGB in the frequency domain, we apply a high-pass filter with a fixed cutoff frequency to the aforementioned three kinds of frequency domain images and convert the filtered results back to the spatial domain. We calculate the Structural Similarity (SSIM) [35] between NIR images and noisy RGB images as well as clean RGB images at different cutoff frequencies as a measure of frequency domain correlation  $S$ , as shown in Fig. 3a. The process can be described as

$$S = \text{SSIM}(\mathcal{F}^{-1}(\mathcal{H}(F_{target})), \mathcal{F}^{-1}(\mathcal{H}(F_{gt}))), \quad (1)$$

where  $\mathcal{F}^{-1}$  denote 2D-IDFT operations,  $F_{target}$  and  $F_{gt}$  represent NIR or noisy RGB and clean RGB after 2D-DFT transformation.  $\mathcal{H}$  represents the filtering of the input image with a high-pass filter. We find that: in the main energy frequency, the image similarity between the input noisy RGB and clean RGB images decreases from low to high frequencies, while the image similarity between the input NIR image and clean RGB image increases from low to high frequencies. More NIR-RGB paired data also exhibit the same correlation (see supplementary materials). Fig. 3b also clearly shows that for noisy RGB images, their high-frequency information is mainly composed of noise



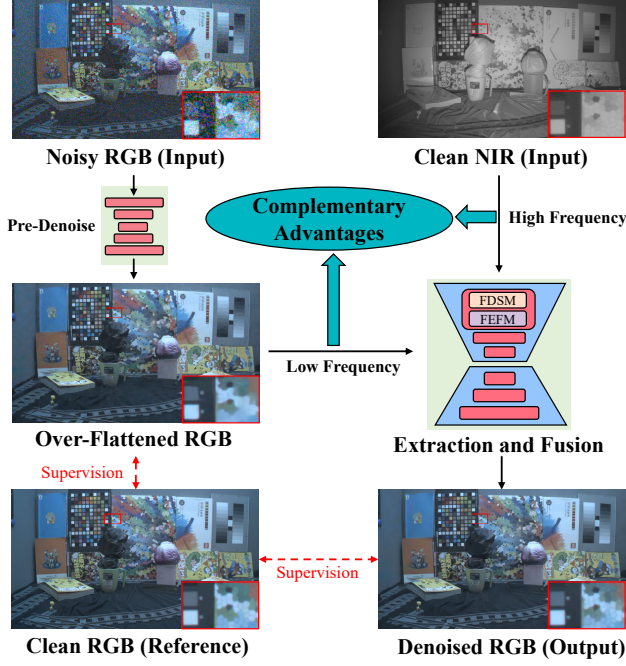


Figure 4. The overall architecture of the proposed cross-field Frequency Correlation Exploiting Network (FCENet).

and lacks detail information, while the low-frequency information more faithfully reflects the color information in the original image, and the NIR image is just the opposite. These cross-field Frequency correlation priors indicate that distinguishing useful information from NIR and RGB image inputs in the frequency domain is simple and efficient, which prompts us to propose a comprehensive frequency domain learning framework.

### 3.2. Overview Framework

The proposed frequency domain fusion framework, as depicted in Fig. 4, includes two stages for the gradual restoration of images. Both stages incorporate an encoder-decoder architecture based on the U-Net [25], featuring two down-sampling layers and two upsampling layers. Skip connections are employed between the encoder and decoder features. A Supervised Attention Module (SAM) [43] is utilized to connect features from the first stage to the second stage for further processing.

In the first stage, the input noisy RGB image undergoes preliminary denoising to reduce the modality gap with the NIR image. In the second stage, we perform multi-scale fusion of the encoded features of the NIR and RGB images. Specifically, at each scale of the encoder, NIR encoded features and RGB pre-denoise features are fed into the frequency domain fusion modules based on FDSM and FEFM, as shown in Fig. 5.

### 3.3. Frequency Dynamic Selection Mechanism

The frequency correlation prior makes us realize that extracting cross-field complementary information from the frequency domain is efficient. For feature extraction, traditional convolutional kernels share weights across the entire feature map, lacking flexibility to address the numerous inconsistencies in NIR and RGB images, which affects the efficiency of extraction. We introduce frequency domain dynamic convolution to adapt to specific inputs and effectively filter out complementary features.

Specifically, given the NIR features  $\mathbf{N} \in \mathbb{R}^{C \times H \times W}$  and pre-denoised features  $\mathbf{R} \in \mathbb{R}^{C \times H \times W}$ , we concatenate them after layernorm and undergo convolution and the activate function to obtain a coarsely fused feature map. After that, we separate the fused feature map to obtain the aggregated features  $\mathbf{A}_R$  and  $\mathbf{A}_N$  for NIR and RGB individually. These aggregated features are used to generate dynamic filtering kernels to selectively extract useful features from the NIR and RGB input features.

For dynamic filters, some works [23, 48] that generate deep separable and spatially variant dynamic filtering kernels are usually computationally intensive and time-consuming, and require a large amount of data. We employed a method similar to [5, 29] by generating dynamic weights to dynamically aggregate multiple parallel convolutional kernels related to the input, and performing this process in the frequency domain. Specifically, the aggregated features  $\mathbf{A}_R$  and  $\mathbf{A}_N$  are used to generate the weights for  $k$  learnable frequency domain filter bases. For each feature channel, these filter bases are linearly combined to form a frequency domain global filter, which is used to select useful frequency domain information from the input NIR and RGB features. Finally,  $\mathbf{F}_R$ ,  $\mathbf{F}_N$  denoting the filtered useful features of NIR and RGB can be represented as

$$\mathbf{DF}_I = \text{Softmax}(\text{MLP}(\text{Pooling}(\mathbf{A}_I))) \cdot \mathbf{G}, \quad (2)$$

$$\mathbf{F}_I = \mathcal{F}^{-1}(\mathcal{F}(\mathbf{I}) \odot \mathbf{DF}_I), \quad (3)$$

where  $\mathbf{DF}_I$  is frequency domain dynamic filter, and  $\mathbf{I}$  represents  $\mathbf{R}$  or  $\mathbf{N}$ .  $\mathbf{G} \in \mathbb{R}^{M \times k}$  represents the combination of  $k$  learnable frequency domain filtering kernels, and  $M$  is the spatial dimension of the convolutional kernel.  $\mathcal{F}$  and  $\mathcal{F}^{-1}$  denote the 2D-DFT and 2D-IDFT operations, respectively.

### 3.4. Frequency Exhaustive Fusion Mechanism

After the NIR and RGB feature maps pass through the Frequency Domain Selection Module (FDSM), the useful features are retained. Next, in order to fuse the two inconsistent fields, we further integrate the information of the two fields in the frequency domain under the incentive of previous frequency domain correlations. Specifically, our Frequency Exhaustive Fusion Mechanism (FEFM) includes two key components: Common Feature Reinforcement Mechanism

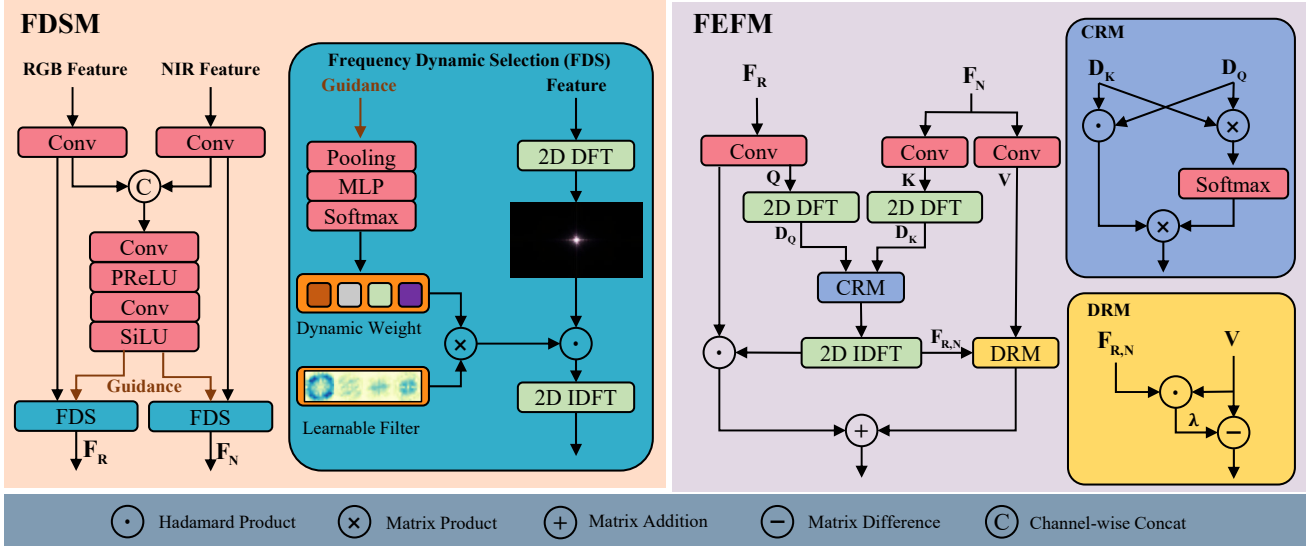


Figure 5. The architecture of the proposed Frequency Dynamic Selection Mechanism (FDSM) and Frequency Exhaustive Fusion Mechanism (FEFM) for thorough frequency exploitation.

(CRM) and Differential Feature Reinforcement Mechanism (DRM). CRM comprehensively explores the correlation between NIR and RGB features in the frequency domain to strengthen the modeling of common features, while DRM employs differential modeling to enhance key differential high-frequency features.

#### Common feature Reinforcement Mechanism (CRM).

The convolution theorem establishes that the correlation or convolution of two signals in the spatial domain is equal to their Hadamard product in the frequency domain. Leveraging this property, previous work [18] integrate the frequency domain into the self-attention mechanism, simplifying matrix multiplication into lightweight element-wise dot product operations. Although the dot product is efficient, it only calculates the point-wise correlation coefficients in the frequency domain, missing the long-range correlations in the frequency domain. To more comprehensively model the common features of NIR and RGB, We apply a point-wise convolution and a depthwise convolution to the input NIR and RGB feature maps  $F_R, F_N$ , to obtain encoded features  $Q=W_d^Q W_p^Q F_R, K=W_d^K W_p^K F_N, V=W_d^V W_p^V F_N$ . To facilitate the calculation of frequency domain correlations, we apply 2D-DFT to the input features to produce frequency cubes  $D_Q$  and  $D_K$ . We simultaneously modeled the long-range correlations and point-wise correlation coefficients of NIR and RGB features in the frequency domain, resulting in a correlation map that integrates local similarities and long-range channel correlations within the frequency domain. The output of CRM can be represented as

$$O_{CRM} = (D_Q \odot D_K) \cdot \text{Softmax}(D_Q \cdot D_K^T / \alpha), \quad (4)$$

where  $\alpha$  is a learnable scaling parameter.

#### Differential feature Reinforcement Mechanism

(DRM). Traditional cross-attention [13, 21, 34] structures are typically used to capture common features but do not effectively utilize differential information. Although this approach is correct in general image fusion frameworks, in this paper, the features of the two fields are considered useful after passing through the frequency domain selection module. By observing the feature maps (Fig. 9), we find that the high-frequency texture information in the NIR features is clear compared to the RGB feature maps. The common features obtained by weighted fusion through cross-attention remain somewhat blurry, which greatly affects the denoising effect. These differential high-frequency features on NIR are crucial for image restoration. We adopt a differential cross-attention to complement the missing differential information, and the output of CRM can be represented as

$$O_{DRM} = (V - \lambda V \odot F^{-1}(O_{CRM})), \quad (5)$$

where  $\lambda$  is a learnable scalar that dynamically controls the weights of two feature maps. Although DRM effectively models the differential high-frequency information, the fused features lack a significant amount of common features and background information. To further refine the fused features, we perform a dot product between the encoded features  $Q$  and the output of CRM, and add the result to the output of DRM as the final fused result.

### 3.5. Loss Function

The setting of the loss function is similar to DVN, adopting the Charbonnier loss [4], and adding a frequency domain

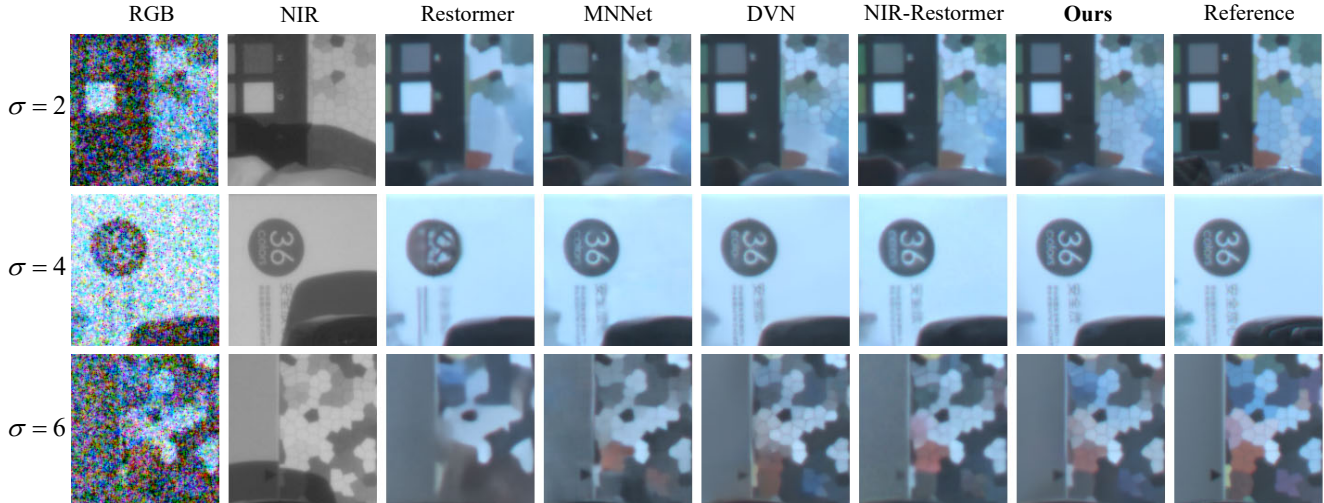


Figure 6. The qualitative comparison among our FCENet and the state-of-the-art methods on the noisy RGB-NIR pairs from DVD[16] with different noise levels. Our method achieves better results in detail recovery, artifact removal, and color restoration.

Table 1. Comparison of different methods on the DVD test set with noise levels  $\sigma = 2, 4, 6$ . The best and second-best results are highlighted in boldface and underlined, respectively.

Methods	$\sigma = 2$		$\sigma = 4$		$\sigma = 6$		Complexity	
	PSNR $\uparrow$	SSIM $\uparrow$	PSNR $\uparrow$	SSIM $\uparrow$	PSNR $\uparrow$	SSIM $\uparrow$	FLOPs(G)	Params(M)
Uformer (CVPR 2022)	31.34	0.949	29.12	0.927	27.58	0.908	9.60	20.63
Restormer (CVPR 2021)	31.30	0.949	29.20	0.928	27.76	0.910	36.06	26.13
MPRNet (CVPR 2021)	31.78	0.951	29.37	0.929	27.84	0.910	133.51	15.74
Xformer (ICLR 2024)	31.41	0.950	29.30	0.928	27.43	0.908	39.34	25.22
CUNet (TPAMI 2020)	28.76	0.923	26.81	0.898	25.64	0.875	<u>6.72</u>	<b>0.44</b>
SANet (CVPR 2023)	30.13	0.938	27.84	0.917	26.41	0.901	25.01	5.38
MNNet (IF 2022)	30.14	0.944	28.26	0.923	26.75	0.906	10.97	<u>0.76</u>
DVN (AAAI 2022)	31.50	0.955	29.62	0.940	28.26	0.927	48.30	6.97
NIR-Restormer (arXiv 2024)	31.81	0.957	29.81	0.942	28.31	0.928	45.31	30.26
FCENet-L (Ours)	<u>31.87</u>	<u>0.960</u>	<u>29.91</u>	<u>0.946</u>	<u>28.36</u>	<u>0.934</u>	<b>5.71</b>	1.16
<b>FCENet (Ours)</b>	<b>32.43</b>	<b>0.963</b>	<b>30.37</b>	<b>0.950</b>	<b>28.78</b>	<b>0.939</b>	19.52	4.32

loss [8]. The overall loss function is represented as

$$\mathcal{L} = \mathcal{L}_{\text{charbonnier}}(\hat{T}_1, G) + \mathcal{L}_{\text{charbonnier}}(\hat{T}_2, G) + \alpha \cdot \mathcal{L}_{\text{charbonnier}}(\mathcal{F}(\hat{T}_1), \mathcal{F}(G)), \quad (6)$$

where  $\hat{T}_1$  and  $\hat{T}_2$  are the outputs of pre-denoising sub-network and whole network, respectively.  $G$  is ground truth and  $\alpha$  is set as 0.1.

## 4. Experiments

In this section, we evaluate our method on public datasets and compare it with other NIR-assisted RGB image denoising methods.

### 4.1. Experimental Settings

**Datasets.** We evaluate the NIR-guided RGB image denoising method on the DVD [16] and IVRG [3] datasets. The DVD dataset consists of 307 high-resolution NIR-RGB image pairs, which are converted into 5k image pairs of size  $3 \times 256 \times 256$  for training and 1k image pairs of size  $3 \times 256 \times 256$  for testing. The IVRG dataset contains NIR and RGB image pairs from 9 different scenes, including countryside, fields, forests, indoors, mountains, old buildings, streets, cities, and water. For each scene, as in [39], experiments randomly select 30/8/15 pairs for training/validation/testing.

**Parameter settings.** The proposed network is trained using the Adam optimizer [11] ( $\beta_1 = 0.9$ ,  $\beta_2 = 0.999$ ) on patches of size  $128 \times 128$  with a batch size of 16. For the



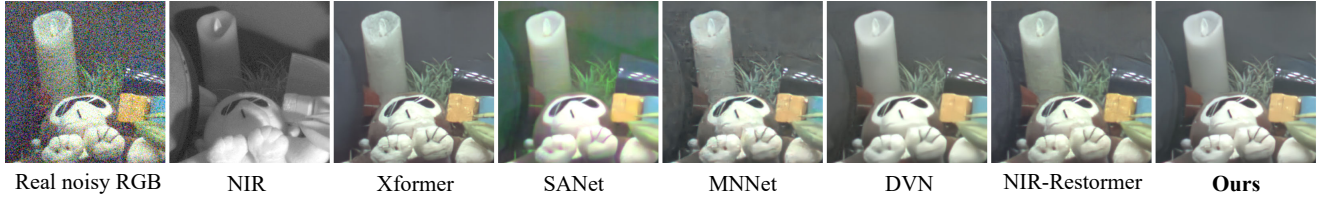


Figure 7. Visual comparisons on real-world RGB/NIR image pairs. Our method demonstrates better visual results.

Table 2. Comparison of different methods on the IVRG test set with noise levels  $\sigma = 25, 50, 75$ . The best and second-best results are highlighted in boldface and underlined, respectively.

Methods	$\sigma = 25$		$\sigma = 50$		$\sigma = 75$	
	PSNR $\uparrow$	SSIM $\uparrow$	PSNR $\uparrow$	SSIM $\uparrow$	PSNR $\uparrow$	SSIM $\uparrow$
Restormer	31.72	0.876	27.67	0.788	24.50	0.722
Uformer	31.97	0.878	27.83	0.793	24.58	0.726
MPRNet	31.89	0.878	27.80	0.794	24.57	0.729
Xformer	31.98	0.879	27.86	0.794	24.61	0.731
CUNet	31.37	0.876	27.78	0.812	24.64	0.764
SANet	31.54	0.885	28.13	0.825	24.81	0.785
MNNet	32.59	0.904	28.66	0.851	25.25	0.808
DVN	32.76	0.906	28.73	0.852	25.28	0.809
NIR-Restormer	<u>32.86</u>	0.906	28.77	0.853	25.30	0.811
FCENet-L (Ours)	32.85	<u>0.909</u>	<u>28.80</u>	<u>0.857</u>	<u>25.33</u>	<u>0.816</u>
<b>FCENet (Ours)</b>	<b>33.26</b>	<b>0.915</b>	<b>29.08</b>	<b>0.866</b>	<b>25.48</b>	<b>0.826</b>

DVD dataset, we simulate low-light conditions by randomly reducing the mean of the original images as in [16] and add Gaussian-Poisson mixed noise with a range of 1 to 16. The model is trained for 80 epochs. The initial learning rate is  $2 \times 10^{-4}$ , and a cosine annealing strategy is used to gradually reduce the learning rate to  $1 \times 10^{-6}$ . For the IVRG dataset, following the settings in [39], it is cropped into 16,374 training patches, and then additive Gaussian noise with random noise levels is used to simulate the target images, considering three noise levels in testing:  $\sigma = 25, 50$ , and 75. The model is trained for 100 epochs with an initial learning rate of  $5 \times 10^{-4}$ . All models are implemented using PyTorch on an NVIDIA RTX 3090 GPU.

## 4.2. Experimental Results

In our experimental evaluation of our method, we compare our results with nine models, including five state-of-the-art NIR-assisted RGB denoising methods: CUNet [10], SANet [27], MNNet [39], DVN [16], and NIR-restormer [38], and four state-of-the-art single-image denoising methods: MPRNet [43], Restormer [44], Uformer [36], and Xformer [45]. To further demonstrate the superiority of our method, we additionally provide the denoising results of a light version (-L) by changing the initial feature map channel count from 64 to 36, which has only 1.16 M parameters. All compared methods are trained on the same training set as ours.

**Evaluations on the DVN dataset.** We first evaluate our

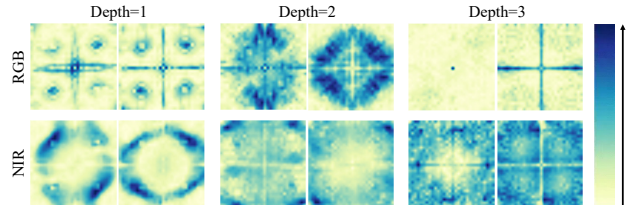


Figure 8. Frequency domain dynamic filters on NIR and RGB side at different depths. The first row represents the frequency-domain filters of RGB side, and the second row represents the filters of NIR side.

method on the DVD dataset, with quantitative results shown in Table 1. It can be observed that our FCENet, and even FCENet-L, outperform all other single-image denoising methods and NIR-assisted denoising methods in terms of PSNR and SSIM with moderate computational and memory costs. The qualitative comparison in Fig. 6 clearly illustrates that our method has a significant advantage over other state-of-the-art methods in noise removal, color preservation, and detail recovery. For single-image denoising methods like Restormer, although they have achieved advanced denoising effects in low-noise scenarios, they still lack effective means to address detail texture loss in high-noise situations. For guided denoising methods, MNNet is unable to effectively handle the significant inconsistencies between NIR and RGB. DVN strengthens consistent high-frequency textures but loses critical differential high-frequency information in NIR and sacrifices the authenticity of low-frequency color; NIR-restormer has good denoising effects but lacks effective utilization of inconsistent information, leading to over-smoothing and color distortion. Our method recovers detailed texture information while more faithfully preserving low-frequency color information in RGB. This proves that our proposed method, through a series of frequency domain learning, can fully exploit useful information from two fields and better solve the fusion problem under the inconsistency of color and structure between NIR and RGB images.

**Evaluations on the IVRG dataset.** We evaluate our method on the IVRG dataset. Following the previous method, we consider three noise levels in the test, including  $\sigma = 25, 50$ , and 75. Quantitative results are shown in Table 2. It can be observed that compared to the state-of-the-art single-image denoising algorithms, our method significantly improves the performance of image denois-

Table 3. Ablation study of various components of our method.

	Baseline	FDSM	FEFM	PSNR↑	SSIM↑
(a)	✓			29.13	0.936
(b)	✓	✓		29.64	0.944
(c)	✓		✓	29.96	0.947
(d)	✓	✓	✓	<b>30.37</b>	<b>0.950</b>

Table 4. Ablation on the branches of FDSM.

Methods	PSNR↑	SSIM↑
w/o FDSM	29.96	0.947
Spatial Dynamic Selection	30.11	0.948
Frequency Dynamic Selection	<b>30.37</b>	<b>0.950</b>

Table 5. Ablation on the branches of FEFM.

Methods	PSNR↑	SSIM↑
Sum	29.64	0.944
Cross-attention	29.85	0.946
DRM	30.15	0.948
DRM + CRM	<b>30.37</b>	<b>0.950</b>

ing, demonstrating the effectiveness of near-infrared images. Compared to existing NIR-assisted denoising methods, our method also has significant advantages. More visualization results are placed in the supplementary material. **Evaluations on real-world experiment.** To further evaluate the performance of our model in real noisy environments, we conduct qualitative experiments on NIR-RGB data pairs in real low-light conditions. As shown in Fig. 7, the introduction of NIR images brings more detailed textures but also a large amount of inconsistency. SANet fails to handle inconsistencies, resulting in a significant amount of artifacts, while MNNet, DVN and NIR-Restormer are unable to thoroughly denoise. In contrast, our method produces a smoother and more natural effect, eliminating inconsistencies while introducing more detailed information.

### 4.3. Ablation Study

We conduct ablation studies on the DVD dataset using our model. The ablation experiments are evaluated under the condition of  $\sigma = 4$ . We first compare the two mechanisms proposed in this paper with a two-stage U-Net baseline, with the results shown in Table 3. In the U-Net baseline, cross-field images are fused through addition. By deploying FDSM and FEFM, the model achieve gains of 0.51dB and 0.83dB, respectively. Finally, combining all contributions significantly improve the denoising level compared to the baseline.

**Effect of FDSM.** Using FDSM allows for better extraction of complementary information from NIR and RGB while handling inconsistent regions. In Fig. 8, we show the frequency domain dynamic filter kernels in FDSM. It

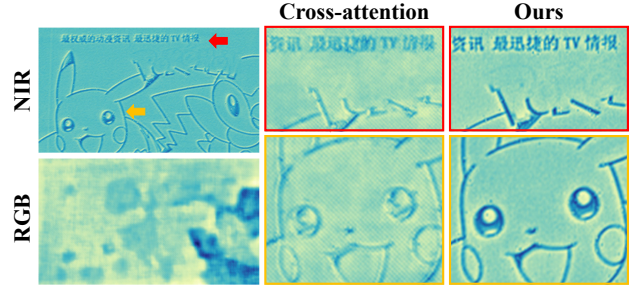


Figure 9. Feature maps obtained from two fields. The first column represents the input feature maps of NIR and RGB, the second column represents the output feature of cross-attention, and the third column is the output feature of FEFM.

can be observed that the filter kernels processing NIR feature maps regularly enhance the learning of mid-to-high frequency information, while those processing RGB feature maps mainly learn low frequency information from the input images. This is consistent with the conclusions drawn from our frequency domain correlation priors. Additionally, we conducted experiments using spatial dynamic convolution in this module. The results in Table 4 ultimately prove the effectiveness of extracting relevant features from the frequency domain in NIR and RGB images and the stability of dynamic convolution in extracting inconsistent features.

**Effect of FEFM.** Traditional cross-attention fusion modules only strengthen common features but neglect differential features. FEFM module strengthens the learning of common features and enhances the learning of some high-frequency differential information in NIR feature maps. Fig. 9 shows the input NIR and RGB feature maps after frequency domain selection, the fused feature maps after cross-attention fusion, and the fused feature maps after FEFM. Compared to the NIR feature maps, the input RGB feature maps still lack significant high-frequency features. It can be seen that our FEFM strengthens common features while supplementing some differential texture information from NIR. We compare two mechanisms in FEFM, the Common feature Reinforcement Mechanism (CRM) and the Differential feature Reinforcement Mechanism (DRM), with traditional cross-attention fusion modules and direct feature summation. The results in Table 5 prove effectiveness of our method in strengthening common features in frequency domain and modeling differential features.

## 5. Conclusion

In this paper, we propose a cross-field frequency correlation exploiting network for NIR-assisted image denoising, termed FCENet. Specifically, we first conduct a series of analyses on the characteristics of NIR and RGB images in frequency domain and obtain frequency correlation prior. Based on the prior, our frequency dynamic selection mechanism dynamically extracts complementary information from cross-field images in the frequency domain, and



we develop a frequency exhaustive fusion mechanism to enhance common features and differential high-frequency features of two fields during fusion process. Extensive experiments on public NIR-RGB datasets demonstrate effectiveness of frequency domain learning, and our method achieves better results than state-of-the-art methods.

## References

- [1] Abdelrahman Abdelhamed, Mahmoud Afifi, Radu Timofte, and Michael S Brown. Ntire 2020 challenge on real image denoising: Dataset, methods and results. In *Proceedings of the IEEE/CVF Conference on Computer Vision and Pattern Recognition Workshops*, pages 496–497, 2020. 1, 2
- [2] Saeed Anwar and Nick Barnes. Real image denoising with feature attention. In *Proceedings of the IEEE/CVF International Conference on Computer Vision*, pages 3155–3164, 2019. 2
- [3] Matthew Brown and Sabine Stüsstrunk. Multi-spectral sift for scene category recognition. In *Proceedings of the IEEE/CVF International Conference on Computer Vision*, pages 177–184, 2011. 6
- [4] Pierre Charbonnier, Laure Blanc-Feraud, Gilles Aubert, and Michel Barlaud. Two deterministic half-quadratic regularization algorithms for computed imaging. In *Proceedings of the International Conference on Image Processing*, pages 168–172, 1994. 5
- [5] Yinpeng Chen, Xiyang Dai, Mengchen Liu, Dongdong Chen, Lu Yuan, and Zicheng Liu. Dynamic convolution: Attention over convolution kernels. In *Proceedings of the IEEE/CVF Conference on Computer Vision and Pattern Recognition*, pages 11030–11039, 2020. 4
- [6] Shen Cheng, Yuzhi Wang, Haibin Huang, Donghao Liu, Haoqiang Fan, and Shuaicheng Liu. Nbnnet: Noise basis learning for image denoising with subspace projection. In *Proceedings of the IEEE/CVF Conference on Computer Vision and Pattern Recognition*, pages 4896–4906, 2021. 2
- [7] Yuxiao Cheng, Runzhao Yang, Zhihong Zhang, Jinli Suo, and Qionghai Dai. A mutually boosting dual sensor computational camera for high quality dark videography. *Information Fusion*, 93:429–440, 2023. 2
- [8] Sung-Jin Cho, Seo-Won Ji, Jun-Pyo Hong, Seung-Won Jung, and Sung-Jea Ko. Rethinking coarse-to-fine approach in single image deblurring. In *Proceedings of the IEEE/CVF International Conference on Computer Vision*, pages 4641–4650, 2021. 6
- [9] Yuning Cui, Yi Tao, Zhenshan Bing, Wenqi Ren, Xinwei Gao, Xiaochun Cao, Kai Huang, and Alois Knoll. Selective frequency network for image restoration. In *International Conference on Learning Representations*, 2023. 3
- [10] Xin Deng and Pier Luigi Dragotti. Deep convolutional neural network for multi-modal image restoration and fusion. *IEEE Transactions on Pattern Analysis and Machine Intelligence*, 43(10):3333–3348, 2020. 2, 3, 7
- [11] P Kingma Diederik. Adam: A method for stochastic optimization. (*No Title*), 2014. 6
- [12] Hansen Feng, Lizhi Wang, Yuzhi Wang, and Hua Huang. Learnability enhancement for low-light raw denoising: Where paired real data meets noise modeling. In *Proceedings of the ACM International Conference on Multimedia*, pages 1436–1444, 2022. 1
- [13] Yuanshen Guan, Ruikang Xu, Mingde Yao, Lizhi Wang, and Zhiwei Xiong. Mutual-guided dynamic network for image fusion. In *Proceedings of the ACM International Conference on Multimedia*, pages 1779–1788, 2023. 5
- [14] Xiaowan Hu, Yuanhao Cai, Jing Lin, Haoqian Wang, Xin Yuan, Yulun Zhang, Radu Timofte, and Luc Van Gool. Hdnet: High-resolution dual-domain learning for spectral compressive imaging. In *Proceedings of the IEEE/CVF Conference on Computer Vision and Pattern Recognition*, pages 17542–17551, 2022. 3
- [15] Liming Jiang, Bo Dai, Wayne Wu, and Chen Change Loy. Focal frequency loss for image reconstruction and synthesis. In *Proceedings of the IEEE/CVF International Conference on Computer Vision*, pages 13919–13929, 2021. 3
- [16] Shuangping Jin, Bingbing Yu, Minhao Jing, Yi Zhou, Jianjun Liang, and Renhe Ji. Darkvisionnet: Low-light imaging via rgb-nir fusion with deep inconsistency prior. In *Proceedings of the AAAI Conference on Artificial Intelligence*, pages 1104–1112, 2022. 1, 2, 3, 6, 7
- [17] Beomjun Kim, Jean Ponce, and Bumsuh Ham. Deformable kernel networks for joint image filtering. *International Journal of Computer Vision*, 129(2):579–600, 2021. 2
- [18] Lingshun Kong, Jiangxin Dong, Jianjun Ge, Mingqiang Li, and Jinshan Pan. Efficient frequency domain-based transformers for high-quality image deblurring. In *Proceedings of the IEEE/CVF Conference on Computer Vision and Pattern Recognition*, pages 5886–5895, 2023. 3, 5
- [19] Tong Li, Hansen Feng, Lizhi Wang, Zhiwei Xiong, and Hua Huang. Stimulating the diffusion model for image denoising via adaptive embedding and ensembling. In *IEEE Transactions on Pattern Analysis and Machine Intelligence (TPAMI)*, pages 8240–8257, 2024. 2
- [20] Jingyun Liang, Jie Zhang Cao, Guolei Sun, Kai Zhang, Luc Van Gool, and Radu Timofte. Swinir: Image restoration using swin transformer. In *Proceedings of the IEEE/CVF international conference on computer vision*, pages 1833–1844, 2021. 1
- [21] Hezheng Lin, Xing Cheng, Xiangyu Wu, and Dong Shen. Cat: Cross attention in vision transformer. In *IEEE International Conference on Multimedia and Expo*, pages 1–6, 2022. 5
- [22] Feifan Lv, Yinqiang Zheng, Yicheng Li, and Feng Lu. An integrated enhancement solution for 24-hour colorful imaging. In *Proceedings of the AAAI Conference on Artificial Intelligence*, pages 11725–11732, 2020. 1, 2
- [23] Ruijun Ma, Shuyi Li, Bob Zhang, and Zhengming Li. Generative adaptive convolutions for real-world noisy image denoising. In *Proceedings of the AAAI Conference on Artificial Intelligence*, pages 1935–1943, 2022. 4
- [24] Ali Rahimi and Benjamin Recht. Random features for large-scale kernel machines. *Advances in Neural Information Processing Systems*, 20, 2007. 3
- [25] Olaf Ronneberger, Philipp Fischer, and Thomas Brox. U-net: Convolutional networks for biomedical image segmentation.

- In *Medical Image Computing and Computer-Assisted Intervention*, pages 234–241, 2015. 4
- [26] Zehua Sheng, Xiongwei Liu, Si-Yuan Cao, Hui-Liang Shen, and Huaqi Zhang. Frequency-domain deep guided image denoising. *IEEE Transactions on Multimedia*, 25:6767–6781, 2022. 2, 3
- [27] Zehua Sheng, Zhu Yu, Xiongwei Liu, Si-Yuan Cao, Yuqi Liu, Hui-Liang Shen, and Huaqi Zhang. Structure aggregation for cross-spectral stereo image guided denoising. In *Proceedings of the IEEE/CVF Conference on Computer Vision and Pattern Recognition*, pages 13997–14006, 2023. 2, 3, 7
- [28] Matthew Tancik, Pratul Srinivasan, Ben Mildenhall, Sara Fridovich-Keil, Nithin Raghavan, Utkarsh Singhal, Ravi Ramamoorthi, Jonathan Barron, and Ren Ng. Fourier features let networks learn high frequency functions in low dimensional domains. *Advances in Neural Information Processing Systems*, 33:7537–7547, 2020. 3
- [29] Yuki Tatsunami and Masato Taki. Fft-based dynamic token mixer for vision. In *Proceedings of the AAAI Conference on Artificial Intelligence*, pages 15328–15336, 2024. 4
- [30] Chunwei Tian, Lunke Fei, Wenxian Zheng, Yong Xu, Wangmeng Zuo, and Chia-Wen Lin. Deep learning on image denoising: An overview. *Neural Networks*, 131:251–275, 2020. 2
- [31] A Vaswani. Attention is all you need. *Advances in Neural Information Processing Systems*, 2017. 1
- [32] Renjie Wan, Boxin Shi, Wenhan Yang, Bihan Wen, Ling-Yu Duan, and Alex C. Kot. Purifying low-light images via near-infrared enlightened image. *IEEE Transactions on Multimedia*, 25:8006–8019, 2023. 1, 2
- [33] Jian Wang, Tianfan Xue, Jonathan T Barron, and Jiawen Chen. Stereoscopic dark flash for low-light photography. In *2019 IEEE International Conference on Computational Photography*, pages 1–10. IEEE, 2019. 2
- [34] Xin Wang, Lizhi Wang, Xiangtian Ma, Maoqing Zhang, Lin Zhu, and Hua Huang. In2set: Intra-inter similarity exploiting transformer for dual-camera compressive hyperspectral imaging. In *Proceedings of the IEEE/CVF Conference on Computer Vision and Pattern Recognition*, pages 24881–24891, 2024. 5
- [35] Zhou Wang, Alan C Bovik, Hamid R Sheikh, and Eero P Simoncelli. Image quality assessment: from error visibility to structural similarity. *IEEE transactions on image processing*, 13(4):600–612, 2004. 3
- [36] Zhendong Wang, Xiaodong Cun, Jianmin Bao, Wengang Zhou, Jianzhuang Liu, and Houqiang Li. Uformer: A general u-shaped transformer for image restoration. In *Proceedings of the IEEE/CVF Conference on Computer Vision and Pattern Recognition*, pages 17683–17693, 2022. 2, 7
- [37] Yunxuan Wei, Shuhang Gu, Yawei Li, Radu Timofte, Longcun Jin, and Hengjie Song. Unsupervised real-world image super resolution via domain-distance aware training. In *Proceedings of the IEEE/CVF conference on computer vision and pattern recognition*, pages 13385–13394, 2021. 3
- [38] Rongjian Xu, Zhilu Zhang, Renlong Wu, and Wangmeng Zuo. Nir-assisted image denoising: A selective fusion approach and a real-world benchmark dataset. *arXiv preprint arXiv:2404.08514*, 2024. 2, 3, 7
- [39] Shuang Xu, Jiangshe Zhang, Jialin Wang, Kai Sun, Chunxia Zhang, Junmin Liu, and Junying Hu. A model-driven network for guided image denoising. *Information Fusion*, 85: 60–71, 2022. 2, 3, 6, 7
- [40] Zhi-Qin John Xu, Yaoyu Zhang, Tao Luo, Yanyang Xiao, and Zheng Ma. Frequency principle: Fourier analysis sheds light on deep neural networks. *arXiv preprint arXiv:1901.06523*, 2019. 3
- [41] Muge Yan, Lizhi Wang, Lin Zhu, and Hua Huang. Exploiting frequency correlation for hyperspectral image reconstruction. *arXiv preprint arXiv:2406.00683*, 2024. 3
- [42] Qiong Yan, Xiaoyong Shen, Li Xu, Shaojie Zhuo, Xiaopeng Zhang, Liang Shen, and Jiaya Jia. Cross-field joint image restoration via scale map. In *Proceedings of the IEEE International Conference on Computer Vision*, pages 1537–1544, 2013. 1, 2, 3
- [43] Syed Waqas Zamir, Aditya Arora, Salman Khan, Munawar Hayat, Fahad Shahbaz Khan, Ming-Hsuan Yang, and Ling Shao. Multi-stage progressive image restoration. In *Proceedings of the IEEE/CVF Conference on Computer Vision and Pattern Recognition*, pages 14821–14831, 2021. 1, 2, 4, 7
- [44] Syed Waqas Zamir, Aditya Arora, Salman Khan, Munawar Hayat, Fahad Shahbaz Khan, and Ming-Hsuan Yang. Restormer: Efficient transformer for high-resolution image restoration. In *Proceedings of the IEEE/CVF Conference on Computer Vision and Pattern Recognition*, pages 5728–5739, 2022. 2, 7
- [45] Jiale Zhang, Yulun Zhang, Jinjin Gu, Jiahua Dong, Linghe Kong, and Xiaokang Yang. Xformer: Hybrid x-shaped transformer for image denoising. *arXiv preprint arXiv:2303.06440*, 2023. 2, 7
- [46] Kai Zhang, Wangmeng Zuo, Yunjin Chen, Deyu Meng, and Lei Zhang. Beyond a gaussian denoiser: Residual learning of deep cnn for image denoising. *IEEE Transactions on Image Processing*, 26(7):3142–3155, 2017. 2
- [47] Kai Zhang, Wangmeng Zuo, and Lei Zhang. Ffdnet: Toward a fast and flexible solution for cnn-based image denoising. *IEEE Transactions on Image Processing*, 27(9):4608–4622, 2018. 1
- [48] Jingkai Zhou, Varun Jampani, Zhixiong Pi, Qiong Liu, and Ming-Hsuan Yang. Decoupled dynamic filter networks. In *Proceedings of the IEEE/CVF Conference on Computer Vision and Pattern Recognition*, pages 6647–6656, 2021. 4
- [49] Wenbin Zou, Mingchao Jiang, Yunchen Zhang, Liang Chen, Zhiyong Lu, and Yi Wu. Sdwnet: A straight dilated network with wavelet transformation for image deblurring. In *Proceedings of the IEEE/CVF International Conference on Computer Vision*, pages 1895–1904, 2021. 3